Review

Research Progress on Sintering Resistance of Ceramic Thermal Protective Coatings

Taotao Cheng *, Peng Chen , Jiayouyu Jiang , Jianhai Yu , Kunying Ding

Posted Date: 28 April 2026

doi: 10.20944/preprints202604.1910.v1

Keywords: ceramic thermal protective coatings; sintering densification resistance; material system innovation; structural optimization; active in-situ pore generation

 doi:10.20944/preprints202604.1910.v1

Article

Research Progress on Sintering Resistance of Ceramic Thermal Protective Coatings

Taotao Cheng [1,2,*], Peng Chen [3], Jiayouyu Jiang [3] and Jianhai Yu [3], Kunying Ding [1,3]

[1] Tianjin Key Laboratory for Civil Aircraft Airworthiness and Maintenance, Civil Aviation University of China, No. 2898, Jinbei Road, Dongli District, Tianjin 300300, China

[2] College of Science, Civil Aviation University of China, No. 2898, Jinbei Road, Dongli District, Tianjin 300300, China

[3] School of Aeronautical Engineering, Civil Aviation University of China, No. 2898, Jinbei Road, Dongli District, Tianjin 300300, China

* Correspondence: ttcheng@cauc.edu.cn

Abstract

Ceramic thermal protective coatings subjected to long-term service in high-temperature environments are prone to internal micro-pore shrinkage, grain coarsening, and collapse of the porous structure, forming a compacted structure. This consequently degrades the durability and safety of the ceramic coatings. This paper elucidated the sintering densification mechanism of ceramic coatings. It analyzed both innovations in material systems and multi-dimensional structural optimization of coatings, summarizing domestic and international research progress on the sintering densification resistance of ceramic coatings. The limitations of traditional techniques that inhibit high-temperature sintering densification through "passive pore retention" were highlighted. A novel approach based on phase transformation-induced pore formation to achieve "active in-situ pore generation" was explored. Building on this, future research directions for enhancing the sintering densification resistance of ceramic thermal barrier coatings were proposed.

Keywords: ceramic thermal protective coatings; sintering densification resistance; material system innovation; structural optimization; active in-situ pore generation

1. Introduction

Ceramic thermal protective coatings were one of the key technologies enabling high thrust-to-weight ratios, efficiency, and longevity in aero-engines. They primarily comprised thermal-insulating ceramic coatings in thermal barrier coating (TBC) systems[1,2], as well as environmental barrier coatings (EBC) and abradable coatings in abradable environmental barrier coating (AEBC) systems[3–6]. Thermal-insulating ceramic coatings were applied primarily to nickel-based/cobalt-based superalloy components, with their core function being high-temperature insulation (reducing substrate temperatures by 100 °C-300 °C). The mainstream material was yttria-stabilized zirconia (YSZ) (featuring low thermal conductivity and high toughness), while novel materials included rare-earth zirconates (higher phase stability), alumina-based coatings (excellent oxidation resistance), and phosphate-based coatings (ultra-low thermal conductivity). Primary fabrication processes were atmospheric plasma spraying (APS) and electron beam physical vapor deposition (EB-PVD). The columnar crystal structure of EB-PVD imparted exceptional thermal cycling resistance to the coatings, making it the preferred technology for engine turbine blades[7]. Abradable environmental barrier coatings (AEBC) were designed specifically for ceramic matrix composites (CMCs, e.g., SiC/SiC) and represented the most complex and advanced thermal protection coatings at that time. The core mission of AEBC was to provide abradable sealing and resist high-temperature water-oxygen corrosion (preventing volatilization of the SiO_2 protective layer into $Si(OH)_4$ gas, which caused substrate degradation). Mainstream materials were rare-earth silicates, including monosilicates (e.g.,

 doi:10.20944/preprints202604.1910.v1

ytterbium silicate, with excellent corrosion resistance), disilicates (e.g., ytterbium disilicate, offering superior thermal matching), and aluminosilicates (possessing self-healing capabilities). The primary AEBC fabrication process was APS, with a development trend toward integration with thermal insulation functions to form thermal/abradable environmental barrier coatings (T/AEBC), supporting next-generation CMC components in ultra-high-temperature environments[8,9]. Through multiple protective mechanisms—including thermal insulation, gas-path sealing, corrosion resistance, and erosion resistance—thermal barrier coatings ensured the safe and reliable operation of engine hot-section components under extreme conditions far exceeding the melting points of substrate materials. They served as an indispensable "protective shield" for modern advanced engines. As engines evolved toward higher temperatures and greater efficiency, particularly with CMCs emerging as the material of choice for advanced engine hot-section components, advanced ceramic thermal barrier coatings featuring ultra-high-temperature resistance (>1500 °C), high performance, multifunctionality, and long service life became a research hotspot in the thermal barrier coating field.

Ceramic thermal barrier coatings were subjected to long-term service in high-temperature (>1000 °C) or ultra-high-temperature environments, causing them to become prone to internal micro-pore shrinkage, grain coarsening, and collapse of columnar crystal structures (e.g., in EB-PVD coatings). This led to the formation of a densified structure, consequently degrading the durability and safety of the coatings through three primary failure mechanisms:① Thermal insulation failure[10,11]: Densification significantly increased thermal conductivity, weakening the core insulating capability. This resulted in overheating of substrate metals or ceramic matrix composites (CMCs), inducing creep, accelerated oxidation, or even melting.② Increased stiffness[12,13]: Elevated rigidity reduced coating toughness and strain tolerance, severely compromising thermal cycling resistance.③ Aggravated internal stress mismatch[14,15]: Tensile stresses generated by sintering shrinkage superimposed with thermal cycling stresses exceeded the coating bonding strength. This initiated microcracks that propagated into macroscopic spallation. Ultimately, these mechanisms caused premature bulk spallation failure of the ceramic coatings.

2. Sintering Densification Mechanism

Sintering densification was one of the primary failure mechanisms in ceramic thermal barrier coatings during high-temperature service. The core reasons driving densification in ceramic materials lay in the significant enhancement of mass transport capability at elevated temperatures and various material transfer mechanisms between particles driven by the minimization of system surface energy. This manifested specifically through: ① Accelerated diffusive mass transfer[16–18]: The rate of diffusive mass transfer generally followed the Arrhenius equation (as shown in equation (1)). For every 100 °C–200 °C temperature increase, the diffusion coefficient rose by 1-2 orders of magnitude. High temperatures (particularly ultra-high temperatures exceeding 1500 °C) dramatically increased atomic/ionic diffusion rates, enabling matter to migrate more readily from particle contact points (high-curvature, high-pressure zones) to necks (low-curvature, low-pressure zones) or along grain boundaries/through bulk diffusion. This filled pores, promoting neck growth and particle center convergence. ② Surface energy-driven densification[19–21]: The fundamental driving force throughout the sintering process was the reduction of total system surface energy (equation (2)). Porous structures possessed substantial solid-gas interfacial energy. High temperatures provided the activation energy required to overcome energy barriers, driving the system spontaneously toward reducing surface area—eliminating pores and enlarging grains—achieving densification through the above mechanisms. ③ Grain adjustment and growth[22,23]: During later sintering stages, grain boundary migration and grain growth (Beck equation, equation (3)) contributed to eliminating small intergranular pores, further increasing density and stiffness.

$$D = D_0 \exp\left(-\frac{E_a}{R\,T}\right) \qquad (1)$$

 doi:10.20944/preprints202604.1910.v1

In Equation (1): D is the diffusion coefficient. D_0 is the pre-exponential factor (related to lattice vibrational frequency). E_a is the diffusion activation energy (energy required to overcome the energy barrier, in J/mol). R is the gas constant (8.314 J/mol·K). T is the absolute temperature (in K).

$$\Delta G = \gamma \cdot \Delta A \qquad (2)$$

In Equation (2):ΔG is the change in Gibbs free energy of the system.γ is the surface tension.

$$G^n - G_0^n = K_0 t \exp\left(-\frac{Q}{RT}\right) \qquad (3)$$

In Equation (3): G is the grain size at time t. G_0 is the initial grain size. n is the grain growth exponent (dimensionless; reflects the dominant mechanism: n = 2 corresponded to ideal grain boundary migration, n = 3 to solute drag or pore pinning, and n = 4 to strong pinning by second-phase particles). t is the holding time. K_0 is the kinetic constant.

3. Research Progress in Sintering Densification Resistance

To break through the high-temperature sintering bottleneck of ceramic coatings, research efforts by domestic and international scholars at that time were concentrated on two primary approaches: ceramic material system optimization and multi-dimensional design of coating structures.

3.1. Material System Optimization

To address structural instability, abnormal grain growth, and uncontrolled densification caused by high-temperature phase transformations (beyond 1175 °C) in conventional yttria-stabilized zirconia (YSZ), international researchers pioneered studies on alternative ceramics like pyrochlore ($Gd_2Zr_2O_7$, GZO) and fluorite ($Eu_2Ce_2O_7$). In 2009, the Japan Fine Ceramics Center[24] investigated the effects of La_2O_3 and HfO_2 doping on the thermal conductivity and thermal cycling life of electron beam physical vapor deposited (EB-PVD) YSZ coatings. These additives were selected for their ability to significantly suppress YSZ sintering. Experiments demonstrated that the developed coatings exhibited both low thermal conductivity and superior sintering resistance. Burner rig tests confirmed that compared to conventional coatings, the novel composition provided enhanced thermal insulation and extended service life. In 2010, Chromalloy Gas Turbine LLC (a global leader in aero-engine TBCs)[25] explored the sintering resistance of a novel TBC material NdxZr1−xOy (where 0<x<0.5, 1.75<y<2, with Z representing Y, Mg, Ca, Hf, or their mixed oxides). NdxZr1−xOy and standard YSZ coatings were fabricated via EB-PVD and atmospheric plasma spraying (APS). Comparative analysis of microstructural evolution pre-/post-sintering in EB-PVD NdxZr1−xOy vs. EB-PVD 7YSZ, alongside characterization of APS NdxZr1−xOy freestanding coatings after 50/100-hour isothermal sintering at 1200 °C, revealed that NdxZr1−xOy coatings outperformed YSZ in sintering resistance for both processes (Figures 1 & 2). In 2016, Darmstadt University of Technology and Forschungszentrum Jülich[26] employed the impulse excitation technique (sensitive to coating stiffness) to evaluate GZO stiffness evolution and sintering behavior. Increased GZO stiffness correlated with microstructural changes: healing of microcracks and sintering of interlamellar cracks/unmelted particles. This revealed that GZO's unique sprayed structure critically governed sintering stability, resulting in distinctive temperature dependence. Above 1300 °C, GZO demonstrated clear advantages over YSZ. In 2018, the Institute of Materials Engineering, Silesian University of Technology[27] synthesized and studied thermal diffusivity of pyrochlore/fluorite-structured europium zirconate, cerate, and hafnate. Results indicated that pyrochlore/fluorite materials exhibited lower thermal diffusivity (slower sintering densification rates) than YSZ at high temperatures. Europium cerate ($Eu_2Ce_2O_7$) emerged as the most promising for thermal insulation, with significantly lower diffusivity above 1000 °C than europium zirconate ($Eu_2Zr_2O_7$) or hafnate ($Eu_2Hf_2O_7$). In 2020, Ondokuz Mayis University[28] conducted isothermal oxidation experiments to analyze hardness and porosity changes in YSZ and $Gd_2Zr_2O_7$ coatings before/after 100-hour oxidation. Post-oxidation, YSZ coatings showed over 100% hardness increase and ~40% porosity reduction, while $Gd_2Zr_2O_7$ coatings had only ~50% hardness rise and ~25% porosity loss. This divergence was

 doi:10.20944/preprints202604.1910.v1

attributed to pyrochlore materials (especially $Gd_2Zr_2O_7$) possessing superior thermal stability and lower elastic modulus than YSZ, thereby effectively inhibiting sintering densification.

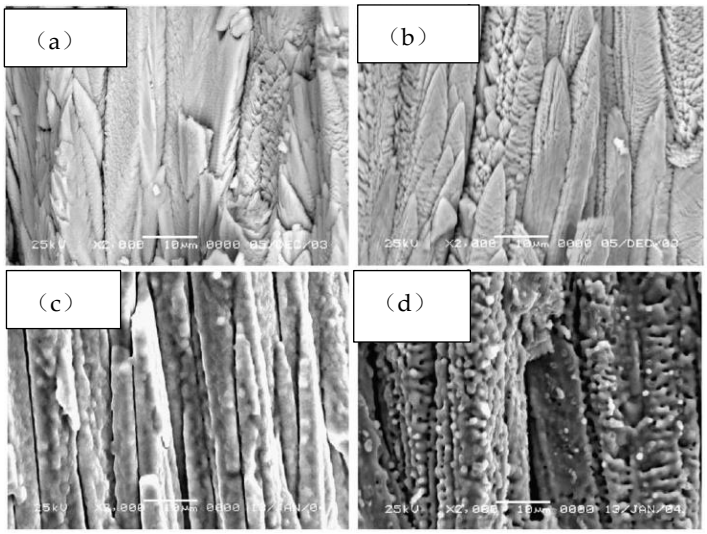

Figure 1. Fracture cross-sectional morphology of EB-PVD deposited NdxZr1−xOy and 7YSZ coatings before and after sintering at 1371 °C for 500 hours[25]: (a) as-deposited 7YSZ; (b) as-deposited NdxZr1−xOy; (c) 7YSZ after sintering; (d) NdxZr1−xOy after sintering.

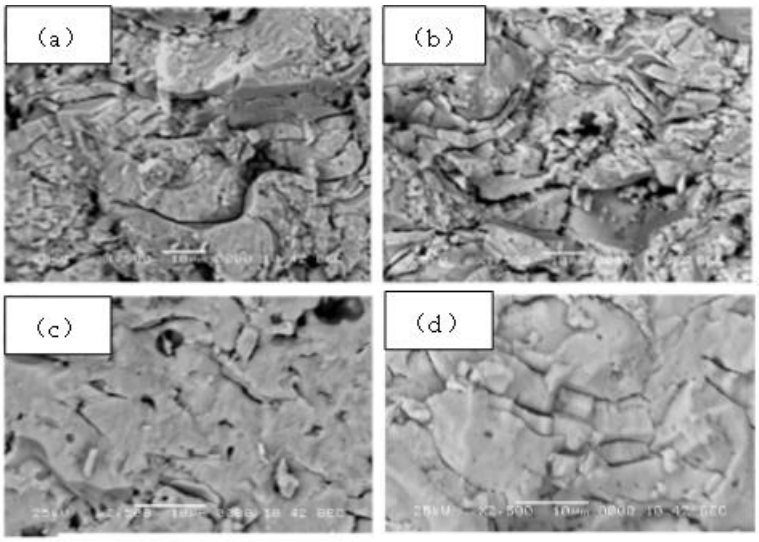

Figure 2. Fracture cross-sectional morphology of APS deposited NdxZr1−xOy and 7YSZ coatings before and after sintering at 1200 °C[25]: (a) as-deposited 7YSZ; (b) as-deposited NdxZr1−xOy; (c) 7YSZ after sintering for 100 hours; (d) NdxZr1−xOy after sintering for 100 hours.

In recent years, domestic scholars also conducted extensive research on optimizing sintering resistance of ceramic materials through compositional design. In 2021, the Lanzhou Institute of Chemical Physics, Chinese Academy of Sciences[29] fabricated CeO_2 and Sc_2O_3 co-doped YSZ ceramic blocks via solid-state sintering. Comparative analysis revealed that CeO_2 doping increased unit cell volume and tetragonality, while Sc_2O_3 doping had the opposite effect. Co-doping induced significant atomic mass/radius disparities and generated abundant oxygen vacancies. These co-doping effects triggered severe lattice distortion and introduced oxygen vacancy defects, effectively suppressing atomic diffusion and enhancing sintering resistance. In 2023, the MOE Engineering Research Center of Nanogeomaterials, China University of Geosciences[30] synthesized a novel high-entropy rare-earth zirconate $(5RE_{0.2})_2Zr_2O_7$ (RE=Dy, Nd, Sm, Eu, Yb) with pyrochlore structure and

 doi:10.20944/preprints202604.1910.v1

superior phase stability via reverse co-precipitation. Benefiting from sluggish diffusion effects, this high-entropy ceramic exhibited exceptional sintering resistance. After annealing at 1600 °C for 1-50 hours, its average grain size increased only from 0.73 μm to 2.22 μm((Figure 3), with a growth rate of ~0.026 $\mu m \cdot h^{-1}$, surpassing traditional pyrochlores. In 2024, Harbin Engineering University[31] achieved targeted design of high-entropy ceramics by regulating ionic disorder and electronegativity differences. Solid-state reactions produced novel multicomponent ceramics $(LaGdYSm)_{x2}Yb_{x1}Zr_2O_7$ ($x_1+4x_2=2$, $x_1=0.6, 0.4, 0.2, 0$). Evaluations showed that increasing radius disorder (δ_r) transformed the structure from pyrochlore/fluorite biphasic to single-phase pyrochlore. The maximum δ_r sample demonstrated the lowest grain growth rate and optimal thermal insulation. In biphasic regions, mutual inhibition of grain growth occurred through lattice distortion and sluggish diffusion. In 2025, the Gas Turbine Research Institute of Shanghai Electric Gas Turbine Co., Ltd.[32] deposited novel $LaMgAl_{11}O_{19}$ (LMA) and YSZ coatings via APS. Static oxidation tests at 1100 °C/1300 °C combined with SEM/XRD characterized porosity, microstructure, and phase evolution. Results indicated that LMA coatings exhibited increasing porosity with prolonged sintering, while YSZ showed significant porosity reduction. LMA underwent rapid phase transformation at high temperatures, forming fine needle-like crystals initially. Extended sintering coarsened these into rod/plate-like structures, enhancing sintering resistance. However, these techniques remained compromised by sacrificed toughness, high costs, and compositional segregation.

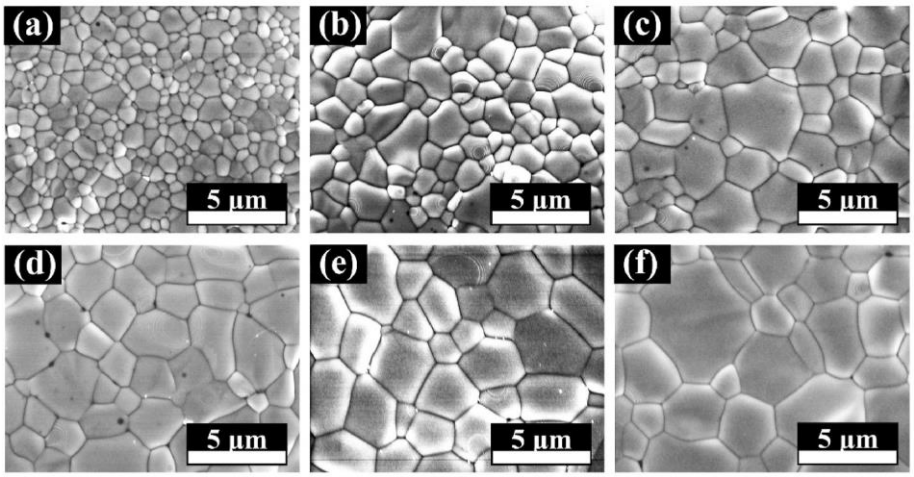

Figure 3. SEM images of $(Dy_{0.2}Nd_{0.2}Sm_{0.2}Eu_{0.2}Yb_{0.2})_2Zr_2O_7$ samples sintered at 1600 °C[30]: (a) 1 hour; (b) 10 hours; (c) 20 hours; (d) 30 hours; (e) 40 hours; (f) 50 hours.

3.2. Multidimensional Design of Coating Structures

Multimodal optimization of ceramic coating structures was established as a critical approach beyond material system innovation to address sintering issues. By regulating structural features such as porosity, pore morphology/distribution, and crack networks, this strategy could reduce mass transport rates and sintering driving forces in high-temperature environments to varying degrees. Consequently, it delayed densification processes while maintaining low thermal conductivity and high strain tolerance of the coatings.

3.2.1. Nano-Bimodal Structural Design

Spray granulation technology was employed to agglomerate nanoparticles into micrometer-sized particles. Through adjustments in the APS process, these agglomerates achieved a gradient melting state: Particle surfaces exceeding 2700 °C melted completely, spreading into lamellar structures upon substrate impact. Ultra-rapid quenching formed dense columnar grains in lamellar zones, simultaneously generating 2D pores and microcracks. Particle cores remained semi-molten at 1600 °C-2000 °C due to thermal lag. Unmelted nano-grains acted as “seeds”, recrystallizing into

 doi:10.20944/preprints202604.1910.v1

equiaxed nano-crystals upon impact to constitute porous nano-zones. The alternating deposition of these structures created a bimodal topology integrating dense lamellar and porous nano-domains. This unique microstructure—featuring dual micron/nano scales within a single phase—contained abundant spherical pores, microcracks, and splats. Compared to conventional coatings, bimodal-structured coatings demonstrated superior sintering resistance.

In 2008, Canada's National Research Council[33] subjected nano-structured and conventional YSZ coatings to 1400 °C heat treatments for 1, 5, and 20 hours. The bimodal microstructure suppressed sintering through two distinct regions: ① A low-sintering-rate matrix layer, ② A high-sintering-rate nano-zone. Critical tests revealed that even after 1400 °C/20-hour exposure, nano-YSZ retained significantly lower thermal diffusivity and elastic modulus than conventional YSZ. This confirmed that structural design enabled nano-YSZ to resist sintering-induced thermal conductivity and modulus increases. The study experimentally established differential sintering kinetics between lamellar and nano-zones, uncovering a "self-compensation effect" whereby high-rate sintering in nano-zones and low-rate sintering in lamellar zones collectively inhibited global densification(Figure 4). This work thus proposed the first mechanistic framework for sintering resistance in ceramic bimodal structures.

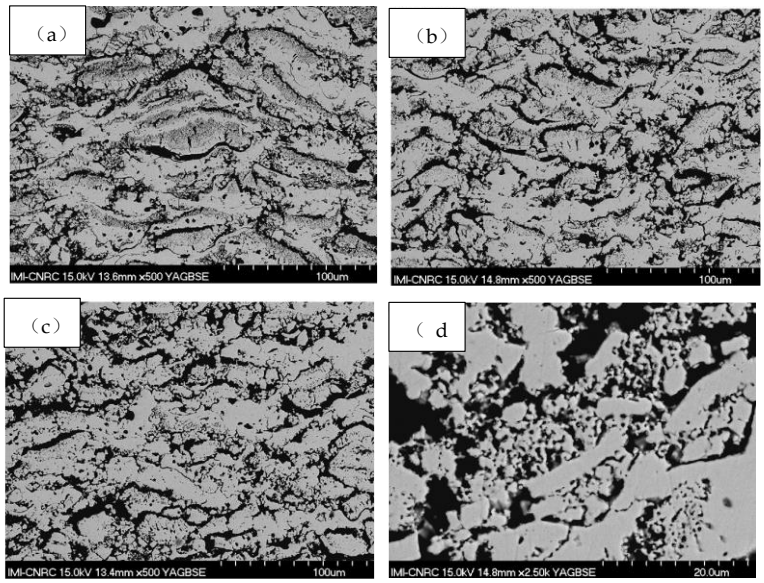

Figure 4. Microstructure (cross-sections) of nano-bimodal structured YSZ coatings after heat treatment at 1400 °C[33]: (a) 1 hour; (b) 5 hours; (c) 20 hours; (d) high-magnification micrograph after 20 hours.

Subsequent research by domestic and international scholars delved deeper into the microstructure and sintering resistance of bimodal-structured ceramic coatings. In 2010, Beihang University[34] fabricated nano-bimodal YSZ coatings via APS. TEM/SEM characterization revealed ~25% porosity in nano-coatings (vs. ~15% in conventional coatings), attributed to abundant inter-splat voids. The nano-coatings exhibited thermal conductivity of 0.8-1.1 W/m·K (≈40% lower than conventional coatings) and surpassed 500 thermal cycles, whereas conventional coatings failed by spallation within 200 cycles. In 2015, Sapienza University of Rome[35] systematically compared thermomechanical properties of APS-YSZ from conventional vs. nano-structured powders. Conventional YSZ showed typical lamellar porous structures with progressive densification, while nano-structured coatings displayed distinct bimodal microstructures (nano-zones + micro-zones). This caused differential sintering: nano-zone densification created peripheral pores, increasing overall porosity. Porosity analysis confirmed opposing trends—conventional coatings decreased porosity with temperature, while nano-structures increased porosity below 1000 °C due to localized densification-induced pore generation. In 2019, Xi'an Jiaotong University[36] investigated sintering behavior of nano-bimodal YSZ. Results indicated superior durability stemmed from distinct sintering

 doi:10.20944/preprints202604.1910.v1

mechanisms: Lamellar zones sintered similarly to conventional coatings via 2D pore healing. Counteractive resistance to 2D pore closure delayed performance degradation. In 2022, Nanchang University[37] deposited YSZ/NiCrAlY bimodal TBCs on Ti-6Al-4V via spark plasma sintering (SPS). This unique structure achieved higher strain tolerance, sintering resistance, and lower thermal conductivity through dense particle contacts and uniformly distributed porous nano-grains. Optimized SPS temperatures extended high-temperature service life. After 100-hour isothermal oxidation at 800 °C, the ceramic topcoat (TC) and bond coat (BC) maintained strong adhesion, with only 6% surface spallation under high-angle bending. However, the high porosity in nano-zones compromised lamellar zone continuity, reducing bonding strength. Random pore aggregation formed "loose channels," accelerating TGO growth and degrading corrosion resistance.

3.2.2. Core-Shell Structural Design

Core-shell structured coatings were constructed by physically encapsulating or chemically synthesizing continuous, dense diffusion-barrier shells on core materials, blocking sintering mass transport pathways at the source to suppress ceramic coating densification. In 2022, Xi'an Jiaotong University[38] developed a nano-porous composite doped with hollow/core-shell fibers featuring high thermal stability and low thermal conductivity, where hollow aerogel matrices significantly reduced solid-phase thermal conductivity while core-shell structures and metal oxide coatings suppressed radiative heat transfer and sintering. In 2024, Xi'an Shiyou University[39] employed dual-feed APS to create mechanically encapsulated "LZO+YSZ+LZO" sandwich-structured powders via collision of solid YSZ with molten $La_2Zr_2O_7$, forming heterogeneous interfaces that inhibited diffusion bridging; results showed powder stream angle variations produced distinct microstructures, and after 1200 °C/200h sintering, conventional YSZ porosity decreased from 31% to 13% (shrinkage ≈4.6%), whereas core-shell variants dropped from 28% to 18% (shrinkage ≈2.4%). In 2024, Northwestern Polytechnical University[40] designed and constructed a nanoscale thermal conduction network with a ceramic@carbon core-shell structure to effectively reduce ablation heat accumulation and enhance the ablation resistance of ZrC-SiC/TaC coatings on carbon/carbon composites. They prepared SiC/TaC encapsulated with graphene shells via the polymer-derived ceramics method and introduced them into ZrC coatings through supersonic atmospheric plasma spraying. The thermally conductive network formed by graphene shells in the coating enhanced heat dissipation capability, lowering the ablation surface temperature by approximately 200 °C. This reduced the volatilization of low-melting-point phases and delayed the sintering of ZrO_2 particles (as shown in Figure 5). In 2025, Central South University[41] synthesized (Ti, Zr, Hf, Ta)CN/SiCN nano-composites via single-source precursor method, with EDS-confirmed uniform elemental distribution and carbon-shell encapsulation effectively inhibiting grain growth. However, both methods faced extreme challenges in uniform encapsulation and introduced interfacial thermal mismatch/elemental interdiffusion that could trigger catastrophic delamination >1300 °C.

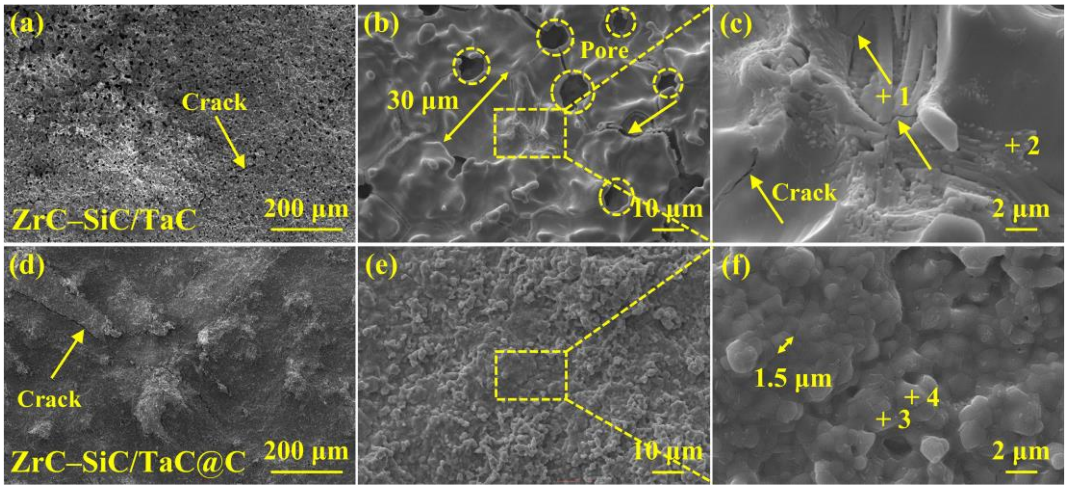

 doi:10.20944/preprints202604.1910.v1

Figure 5. Surface SE images of specimens after ablation for 90 s×2[40]: (a-c) ZrC-SiC/TaC and (d-f) ZrC-SiC/TaC@C.

3.2.3. Pore Structure Design

Pore structure design primarily enhanced sintering resistance through multiscale porosity construction. In 2020, East China University of Science and Technology[42] embedded agglomerated micrometer-sized 8YSZ powders with unique pore structures (unmelted/semi-melted) into conventional coatings, creating composite structures where novel particles uniformly dispersed within the matrix. Microstructural and mechanical analysis systematically investigated failure mechanisms and sintering behavior: conventional APS-YSZ underwent rapid sintering-induced stiffening, with elastic modulus increasing to ≈3× the as-sprayed state within short-term exposure, whereas the novel structure demonstrated exceptional sintering resistance, maintaining strain tolerance comparable to the as-sprayed state even post-thermal shock. Premature failure in conventional coatings was primarily triggered by rapid sintering, while the novel TBC's extended service life was attributed to reduced sintering-driven cracking forces. In 2022, South China University of Technology[43] injected YSZ powders with fine/coarse pores into the plasma plume tail via modified feeding, fabricating porous coatings containing differentially flattened particles with distinct pore architectures (Figure 6). Comparative studies revealed pore morphology's influence on sintering through quasi-in situ observation. Results confirmed that tailored porous unmelted particles significantly improved sintering resistance; micron-scale pores remained structurally stable at high temperatures, resisting sintering-induced healing and preserving low thermal conductivity/stiffness long-term. However, this approach suffered from substantially compromised mechanical properties due to large-scale pores/high porosity and complex process control.

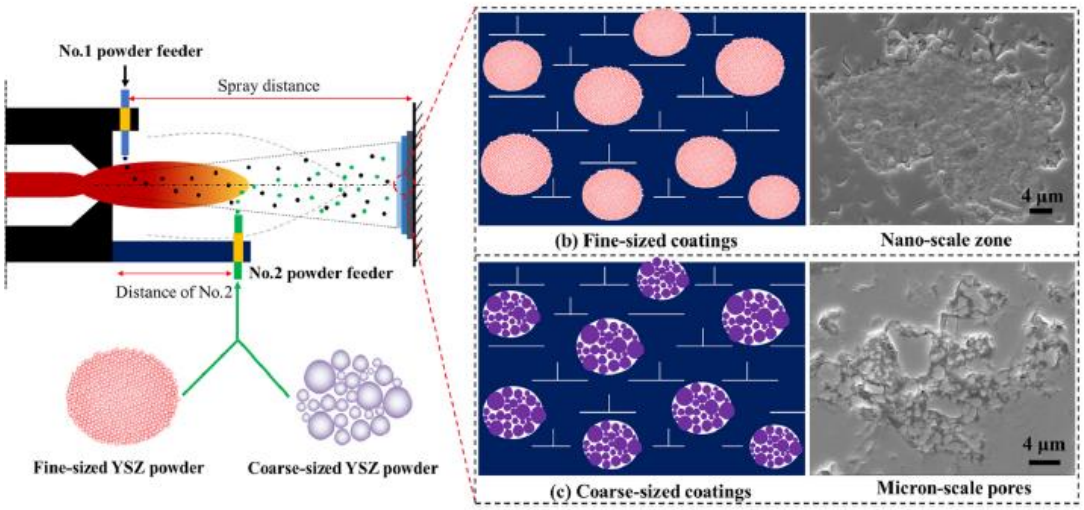

Figure 6. Schematic diagram of composite coating fabrication method and pore structure regulation via fine/coarse powder control[43].

3.2.4. Multilayered Structural Design

Multilayered structural design transformed conventional continuous stacking into bilayer, multilayer, and graded configurations, significantly reducing thermal conductivity and relieving sintering stresses to enhance sintering resistance. In 2012, the Beijing Institute of Aeronautical Materials[44] fabricated $La_2(Zr_{0.7}Ce_{0.3})_2O_7$ (LZ7C3)/YSZ double-ceramic-layer (DCL) TBCs via EB-PVD. At 1573K burner rig tests, DCL achieved 27% longer thermal cycling life than YSZ, attributed to LZ7C3's superior sintering resistance and unique columnar grain growth. In 2016, Universitat Politècnica de València[45] employed dual-feed APS to prepare multilayered/functionally graded

 doi:10.20944/preprints202604.1910.v1

YSZ/$Gd_2Zr_2O_7$ coatings. XRD confirmed only tetragonal ZrO_2 and pyrochlore $Gd_2Zr_2O_7$ phases. Post-annealing, functionally graded structures demonstrated optimal sintering resistance and thermal fatigue performance by synergizing $Gd_2Zr_2O_7$'s low thermal conductivity with graded stress relief. In 2018, Xi'an Jiaotong University[46] proposed gradient structures to counteract sintering. Thermo-mechanical FEA and experiments revealed slower strength/conductivity degradation in compositionally graded porous TBCs. A novel sintering resistance parameter was established to evaluate performance under isothermal/thermal-gradient conditions, proving that TBCs with porosity gradually decreasing from top to bottom exhibited superior sintering resistance. In 2022, Université de Bordeaux[47] determined that optimal environmental barrier coatings (EBCs) require multilayered designs: outer layers of coarse-grained yttrium monosilicate suppressed volatilization while providing thermal insulation; middle layers of submicron yttrium disilicate acted as diffusion barriers, reducing oxidant flux to inhibit bond coat oxidation. This bilayer design lowered operating temperatures in intermediate layers, limiting grain coalescence and ion diffusion. In 2025, East China University of Science and Technology[48] developed Gd/Yb co-doped YSZ (RYSZ) powders, fabricating RYSZ/8YSZ DCL coatings via APS. After 200h at 1150 °C, DCL porosity decreased only 29.89% vs. 73.94% for monolithic 8YSZ. DCL withstood 60 thermal cycles without failure, outperforming monolithic RYSZ (35 cycles) and 8YSZ (40 cycles).

Concurrently (2023–2025), the authors implemented bionic shell-inspired "brick-mud" layered YSZ seal coatings[49–52] using high-temperature adhesives and cyclic APS deposition. Thermal cycling tests demonstrated that low-fracture-toughness "mud" layers induced priority microcracking to relieve sintering stresses (Figure 7), delaying densification and enhancing thermal cycling performance.

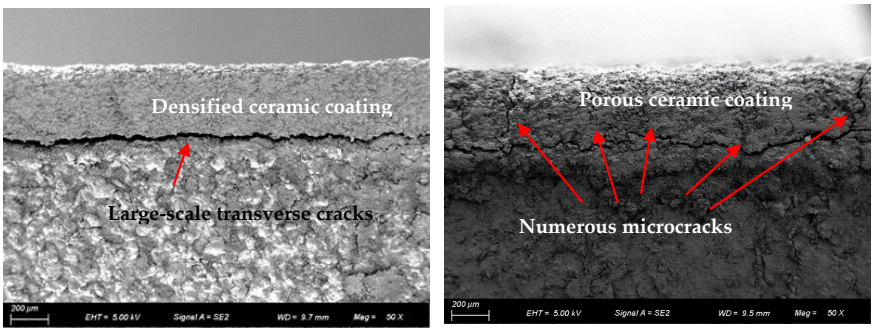

Figure 7. Anti-sintering densification effect of "brick-mud" structured coatings: (a) conventional seal coating;. (b) "brick-mud" structured seal coating.

However, these multilayered structures typically faced critical challenges: interfacial stress concentration, delamination failure due to sintering behavior discrepancies, complex fabrication of multi-interface architectures, and critically challenging process control during manufacturing[48].

3.2.5. Limitations of Existing Technologies

Structural densification manifested as pore reduction and diminished pore size was the most prominent indicator of ceramic coating sintering degradation. Conventional abradable seal coatings (porous ceramics) relied on pre-incorporated pore formers that burned out during service, inevitably suffering sintering densification, stiffness escalation, and high-temperature performance decay at elevated temperatures. This severely compromised abradable rotors and overall engine safety. Earlier domestic and international research passively decelerated porosity loss through material system optimization and multidimensional structural design ("passive pore retention"), achieving notable progress in sintering resistance. However, these anti-sintering mechanisms merely delayed densification rates—their effectiveness diminished with prolonged service time, revealing

 doi:10.20944/preprints202604.1910.v1

fundamental limitations in counteracting ceramic coating densification. Simultaneously, these approaches faced persistent shortcomings as summarized in Table 1, creating an urgent need for innovative anti-sintering strategies in thermal barrier coatings.

Table 1. Key characteristics of current anti-sintering technologies.

Category	Representative technology	Key advantages	Key limitations
Material system innovation	Rare-earth oxide doping	Rare-earth doping intensifies lattice distortion, thereby reducing atomic diffusion rate.	Low fracture toughness, particularly at high dopant concentrations which degrade the ceramic matrix's fracture resistance, coupled with a low coefficient of thermal expansion, this combination severely compromises thermal cycling performance.
	Second-phase introduction	Oxygen vacancy regulation: high vacancy concentration delays densification. Grain boundary pinning: YAG second phases refine grains and thus suppress boundary migration.	High cost: rare-earth oxides (e.g., CeO_2, Sc_2O_3) are prohibitively expensive, consequently limiting scalability.
	High-entropy pyrochlore design	Leveraging the sluggish diffusion effect, high-entropy ceramics demonstrate significantly enhanced sintering resistance.	Complex multi-component solid-state synthesis drives up raw material costs (8-10× higher than YSZ when rare-earth oxide purity exceeds 99.9%), while kinetic imbalances in multi-element diffusion may trigger compositional segregation.
Multidimensional coating structure optimization	Nano-bimodal structure design	The bimodal microstructure incorporates abundant spherical pores, microcracks, and splats, endowing the coating with significantly enhanced sintering resistance.	The high porosity in nano-zones compromises lamellar continuity, reducing bonding strength. Furthermore, random pore aggregation forms "loose channels," accelerating TGO growth and degrading corrosion resistance.
	Core-shell structure design	Heterogeneous interfaces block diffusion bridging between YSZ lamellae, inhibiting mass transport and thereby enhancing sintering resistance.	Achieving uniform encapsulation poses extreme challenges and introduces new failure mechanisms, namely interfacial thermal mismatch and elemental interdiffusion, which could trigger catastrophic delamination in ultra-high-temperature environments (>1300 °C).

 doi:10.20944/preprints202604.1910.v1

	Pore structure design	Micropores buffer stress, nanopores block mass transfer.	Large-scale pores and high porosity substantially reduce mechanical properties while introducing critically challenging process control complexities.
	Multilayered structure design	The bilayer structure provides a low-thermal-conductivity top layer while maintaining high fracture toughness and thermal expansion matching in the bottom layer.	Interfacial stress concentration and sintering behavior discrepancies lead to delamination failure.
		Multilayer structures enable independent parameter design (porosity/composition) per layer while optimizing stress gradients.	The fabrication of multilayer/multi-interface structures involves complex processes and incurs substantially higher costs.
		Graded structures achieve continuous compositional gradients and multifunctional integration, enabling synergistic anti-sintering mechanisms.	Fabrication poses extreme difficulties: elemental interdiffusion at elevated temperatures may cause significant gradient degradation, while the absence of distinct interfaces complicates characterization.
		In the novel “brick-mud” structure, the “mud” layer undergoes prioritized microcracking to release sintering-induced stresses, significantly delaying the densification process.	“Brick-mud” structured coatings involve complex fabrication processes with critically demanding preparation control.

4. Outlook

In 2025, during thermal cycling tests of SiC-substrate abradable environmental barrier coatings (1.5h holding at 1350 °C followed by 0.5h cooling to room temperature), the authors observed distinctive “large-scale chain-like pores” within the Si coating post-failure, as shown in Figure 8(e).

 doi:10.20944/preprints202604.1910.v1

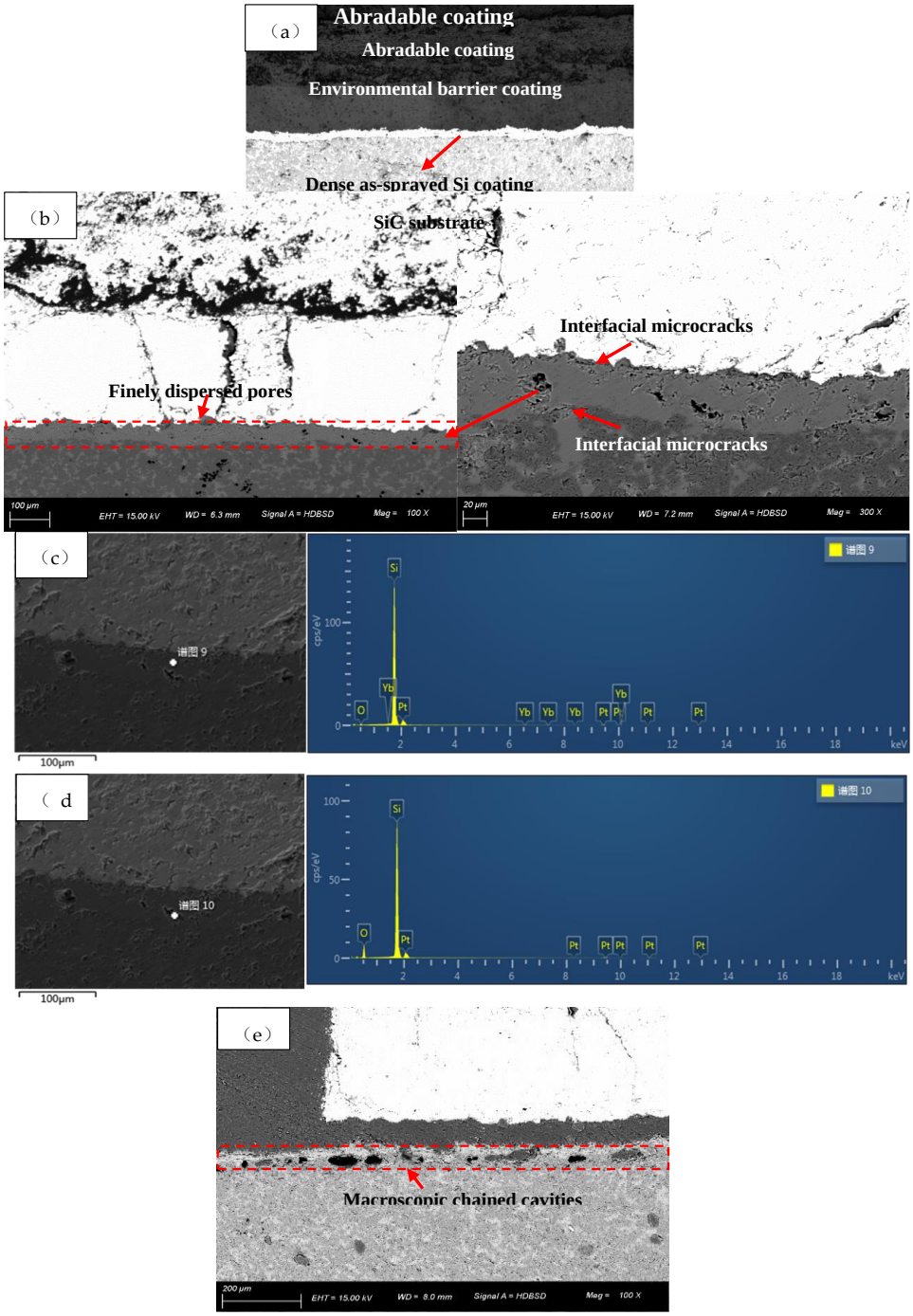

Figure 8. Formation process of "chained cavities" in the Si coating on SiC substrate: (a) As-sprayed coating; (b) cross-sectional morphology of Si coating after 20 thermal cycles; (c) EDS analysis of dense region; (d) EDS analysis of cavity region; (e) cross-sectional morphology of Si coating after 40 thermal cycles.

Figure 8(a) shows the as-sprayed abradable environmental barrier coating. The Si layer functioned as a bond coating to mitigate thermal expansion mismatch, exhibiting a dense structure with minimal porosity. After 20 thermal cycles, Figure 8(b) revealed the emergence of finely dispersed micropores within the Si layer, at the Si/SiC substrate interface, and at the Si/EBC interface. Upon increasing thermal cycles to 40, Figure 8(e) demonstrated significant growth and coalescence of these pores, evolving into macroscopic chained cavities. Combined analysis of Fig.s 8(c) and 8(d) indicated that under thermally induced fatigue stresses and TGO growth-induced stresses (which intensify with increasing TGO thickness), severe cracking occurred not only within the abradable coating and EBC but also prominently within the Si layer and along its interfaces with the SiC

 doi:10.20944/preprints202604.1910.v1

substrate and EBC. Oxygen (O) permeated not only through cracks in the abradable ceramic layer and EBC but also migrated along cracks within the Si layer and interfacial regions. This facilitated direct in-situ reaction between oxygen and the Si layer, accelerating oxidation of the bond coat. Consequently, during thermal cycling, the bond coating comprised a mixture of unoxidized Si and a TGO layer.

The primary reaction between Si and O_2 at 1350 °C formed SiO_2. Upon cooling to approximately 267 °C, this SiO_2 typically crystallized as β-cristobalite (high-temperature polymorph). Subsequent cooling below 267 °C triggered a phase transformation from β-cristobalite to α-cristobalite (low-temperature polymorph), accompanied by 0.9%-1.5% volumetric contraction. This contraction generated primary pores. During reheating, the reverse transformation (α- to β-cristobalite) induced 0.9%–1.5% volumetric expansion. However, due to pre-existing pores, anisotropic expansion, and trapped gases, this expansion failed to fully heal defects and could even enlarge them[53,54]. Ultimately, repeated thermal cycling led to pore accumulation and interconnection, forming the macroscopic chained cavities observed in Figure 8(e).

The reversible $\beta \rightleftarrows \alpha$ cristobalite phase transformation in the Si layer, with its significant cyclic contraction/expansion, drives the nucleation, growth, and accumulation of pores. This mechanism not only offers a novel pore-engineering strategy for porous ceramic coatings but also inspires innovative design approaches to counteract high-temperature sintering-induced densification in ceramic coatings. Based on this analysis, the authors suggest the following research directions merit further investigation:

(1) In-situ active pore-forming technology. During high-to-low temperature cyclic thermal shocks, the polymorphic transformations of ceramic phases are accompanied by significant volumetric contraction or expansion effects. Examples include: Zirconia (ZrO_2): Tetragonal phase (t-ZrO_2) → Monoclinic phase (m-ZrO_2), accompanied by 3%-5% volumetric expansion. Cristobalite (SiO_2): β-cristobalite (high-temperature form) → α-cristobalite (low-temperature form), undergoing 2.8% volumetric contraction. Alumina (Al_2O_3): γ-Al_2O_3 (cubic) → α-Al_2O_3 (hexagonal), resulting in ~15% volumetric contraction. The volumetric contraction process directly generates primary pores. Conversely, during the volumetric expansion phase, pre-existing pores, anisotropic expansion, and trapped gases prevent complete pore healing and may even enlarge defects. Repeated thermal cycling subsequently leads to pore formation and accumulation. This mechanism provides a novel design strategy for achieving “in-situ active pore control” in advanced ceramic coatings, thereby suppressing coating densification.

(2) Composite pore-control technology. In the in-situ pore-forming process, polymorphic ceramic particles undergo reversible phase transitions under thermal cycling. The accompanying cyclic volumetric expansion/contraction continuously induces pore nucleation and growth. Accumulated pores exert a stress-relief effect (e.g., mitigating thermal mismatch stress and phase transformation stress). During this stress-relief process, stored elastic strain energy is converted into a driving force for grain boundary migration. This promotes pore coalescence along grain boundaries and triggers grain growth, ultimately reducing porosity—a detrimental factor for the sintering resistance of ultra-high-temperature abradable coatings. Therefore, building upon the “in-situ active pore-forming” technology, it is imperative to develop effective methods to inhibit porosity reduction and grain growth (e.g., via grain boundary pinning by nanoparticles or nano-bimodal effects). This forms a “composite pore-control” technology. Ultimately, this approach enables the fabrication of novel ultra-high temperature sintering resistant thermal barrier coatings with synergistic pore-forming and pore-stabilizing mechanisms.

Funding: This work was supported by the Natural Science Key Project of Basic Research Funds of Central Universities(3122025081).

 doi:10.20944/preprints202604.1910.v1

References

1. F W Meng, F X Ye, T Y Luo; et al. Unveiling CMAS corrosion mechanism on the surface of a novel mid-entropy Hf-Ta ceramic for thermal barrier coatings[J]. Applied Surface Science, 2025, 702: 163310.
2. J V Kurian; M R Radhakrishna Panicker, P. A. Job; et al. Tailoring structural and thermal properties of neodymium hafnium-zirconium oxide nano particles (Nd2(Hf1-xZrx)2O7; x=0.2, 0.5) for thermal barrier coatings[J]. Nano Express, 2025, 6(3): 035009.
3. N Yamazaki, K Doi, Nakamura, T.; et al. Improvement of CMAS corrosion resistance in ytterbium aluminum garnet by multi-phasing of ytterbium oxide[J]. Journal of the European Ceramic Society, 2025, 45(13): 117474.
4. Z J Zhang, G Jin, X F Cui; et al. Thermomechanical degradation mechanisms of high-entropy (Yb0.25Er0.25Ho0.25Y0.25)2SiO5 environmental barrier coatings under CMAS melt infiltration[J]. Journal of the European Ceramic Society, 2025, 45(15): 117606.
5. T T Cheng, Z P Wang, S J. Dai; et al. Research progress of ceramic-based high temperature sealing coating for aeroengines [J]. Journal of Mechanical Engineering, 2021, 57(10): 126-136+147.
6. A Lynam, R A Romero, B Zhang; et al. Abradable ytterbium disilicate environmental barrier coatings: A story of CMAS and combined CMAS-erosion performance[J]. Surface & Coatings Technology, 2024, 494(P3): 131502.
7. K S Vaiyapuri, A Moganraj, A Nowotnik. High temperature cyclic CMAS corrosion of TBCs on second generation single crystal superalloy deposited using beam switching EBPVD technology[J]. Surface & Coatings Technology, 2025, 507: 132134.
8. A Lynam, B Zhang, R A Romero; et al. Abradable ytterbium disilicate environmental barrier coatings: A study of steam, CMAS and combined steam-CMAS corrosion[J]. Journal of the European Ceramic Society, 2025, 45(14): 117544.
9. A Lynam, R A Romero, F Xu; et al. An investigation into the erosion and wear mechanisms observed in abradable ytterbium disilicate environmental barrier coatings[J]. Journal of the European Ceramic Society, 2024, 44(12): 7310-7327.
10. K H Yang, J M Shi, F Q Tian; et al. Lanthanide co-doped YSZ double-ceramic-layer thermal barrier coatings: Unlocking superior sintering resistance, thermal durability, and insulation for extreme environments[J]. Surface & Coatings Technology, 2025(504): 132069.
11. K Y Li, S Huang, S Zhang; et al. A novel sintering resistant Sr(Eu0.2Ho0.2Er0.2Tm0.2Yb0.2)2O4 high-entropy ceramic with superior thermophysical properties for advanced thermal barrier coatings[J]. Journal of the European Ceramic Society, 2025, 45(2): 116909.
12. Y W Jia, H F Wang, Y D Wang; et al. Research status on thermal barrier coating of aircraft engine turbine blade [J]. Surface Technology, 2023, 52(11): 139-154.
13. H Xie, V K Champagne, W. Zhong; et al. Design, fabrication, and screening of environmental-thermal barrier coatings prepared by ultrafast high-temperature sintering[J]. Advanced Functional Materials, 2023, 34(10): 2309978.
14. B W Lv, C Wang, X F Zhang; et al. Stress-dependent sintering behavior of porous thermal barrier coatings[J]. Journal of the European Ceramic Society, 2023, 43(6): 2634-2645.
15. K Liu, X Chen, K P Du; et al. LC\8YSZ TBCs thermal cycling life and failure mechanism under extreme temperature gradients[J]. Coatings, 2021, 11(9): 1051-1051.
16. C W Wang, W W Ping, Q Bai; et al. A general method to synthesize and sinter bulk ceramics in seconds[J.]. Science (New York, N.Y.), 2020, 368(6490): 521-526.
17. H T Chen, X F Zhang, K S. Zhou; et al. Structure evolution of nano-7YSZ ceramic coating during gradient.
18. thermal cycle [J]. Surface Technology, 2017, 46(06): 256-262.
19. J.; Guo, Y.; Yin, M Yi. Extreme temperature gradient promoting oxygen diffusion in yttria-stabilized zirconia: A molecular dynamics study[J]. Journal of the American Ceramic Society, 2024, 107(10): 6783-6790.
20. J S Du, B H Tang, Y J Lei; et al. Texture grain growth on the surface of 95% alumina ceramic during the sintering and its phase-field simulation [J]. Journal of Synthetic Crystals, 2019, 48(02): 240-247.

 doi:10.20944/preprints202604.1910.v1

21. L S Wang, J B Song, H Dong; et al. Sintering-induced failure mechanism of thermal barrier coatings and sintering-resistant design[J]. Coatings, 2022, 12(8): 12081083.
22. D Gouvêa. Thermodynamic of solid-state sintering: Contributions of grain boundary energy[J]. Journal of the European Ceramic Society, 2024, 44(14): 116677.
23. M R German. Sintering trajectories: Description on how density, surface area, and grain size change[J]. JOM, 2016, 68(3): 878-884.
24. M Zhang, W J Wang, T C Yuan; et al. Densification and grain growth kinetics of boron carbide powder during ultrahigh temperature spark plasma sintering[J]. Transactions of Nonferrous Metals Society of China, 2022, 32(06): 1948-1960.
25. M Matsumoto, T Kato, N Yamaguchi; et al. Thermal conductivity and thermal cycle life of La_2O_3 and HfO 2 doped ZrO_2-Y_2O_3 coatings produced by EB-PVD[J]. Surface & Coatings Technology, 2009, 203(19): 2835-2840.
26. Y L Liu, R Shankar, P Howard. High sintering resistance of a novel thermal barrier coating[J]. Surface & Coatings Technology, 2010, 204(20): 3154-3160.
27. M Frommherz, A Scholz, M. Oechsner; et al. Gadolinium zirconate/YSZ thermal barrier coatings: Mixed-mode interfacial fracture toughness and sintering behavior[J]. Surface & Coatings Technology, 2016, 286: 119-128.
28. M Mikuśkiewicz, G Moskal, D. Migas; et al. Thermal diffusivity characterization of europium zirconate, cerate and hafnate[J]. Ceramics International, 2018, 45(2):2760-2770.
29. K M Doleker, A C Karaoglanli, Y. Ozgurluk; et al. Performance of single YSZ, Gd2Zr2O7 and double-layered YSZ/$Gd_2Zr_2O_7$ thermal barrier coatings in isothermal oxidation test conditions[J]. Vacuum, 2020, 177: 109401.
30. X D Wei, G L Hou, Y L An; et al. Effect of doping CeO_2 and Sc_2O_3 on structure, thermal properties and sintering resistance of YSZ. Ceramics International, 2021, 47(5): 6875-6883.
31. X W Luo, S Huang, R Q Huang; et al. Highly anti-sintering and toughened pyrochlore (Dy0.2Nd0.2Sm0.2Eu0.2Yb0.2)2Zr2O7 high-entropy ceramic for advanced thermal barrier coatings[J]. Ceramics International, 2023, 49(14PA): 23410-23416.
32. Z Chen, X F Cui, Y Z Jing; et al. High temperature performance of $RE_2Zr_2O_7$ high-entropy ceramics designed by thermos physical performance oriented principle[J]. Ceramics International, 2024, 50(9PB): 16499-16510.
33. L.; He, T T Deng. Comparison of sintering resistance property of new thermal barrier coatings LaMgAl11O19 and YSZ coatings for heavy-duty gas turbines[J]. Journal of Materials Engineering, 2025, 53(03): 159-168.
34. R.; Lima, B Marple. Nanostructured YSZ thermal barrier coatings engineered to counteract sintering effects[J]. Materials Science & Engineering A, 2008, 485(1-2): 182-193.
35. J Wu, H B Guo, L Zhou; et al. Microstructure and thermal properties of plasma sprayed thermal barrier coatings from nanostructured YSZ[J]. Journal of Thermal Spray Technology, 2010, 19(6): 1186-1194.
36. L Baiamonte, F Marra, G. Pulci; et al. High temperature mechanical characterization of plasma-sprayed zirconia–yttria from conventional and nanostructured powders[J]. Surface & Coatings Technology, 2015: 277, 289-298.
37. G. R.; Li, G J Yang. Understanding of degradation-resistant behavior of nanostructured thermal barrier coatings with bimodal structure[J]. Journal of Materials Science & Technology, 2019, 35(03): 231-238.
38. C Jiang, J Chen, Z H Zhu. Novel structured spark plasma sintered thermal barrier coatings with high strain tolerance and oxidation resistance[J]. Ceramics International, 2022, 48(9): 12271-12280.
39. Xi'an Jiaotong University. A nanoporous composite material doped with hollow/core-shell fibers exhibiting high thermal stability and low thermal conductivity: 202211324167.4[P]. 2023-01-06.
40. Xi'an Shiyou University. An anti-sintering thermal barrier coating based on dual-shell microstructured composite ceramic powder and preparation method thereof: 202410186273.3[P]. 2024-05-07.
41. Y Y Zhang, X M Zhang, H K Ou; et al. Heat dissipation of carbon shell in ZrC–SiC/TaC coating to improve protective ability against ultrahigh temperature ablation[J]. Journal of Advanced Ceramics, 2024, 13(7): 1080-1091.

 doi:10.20944/preprints202604.1910.v1

42. T X Jiang, Q B Wen, L Lu; et al. (Ti, Zr, Hf, Ta)CN/SiCN: A new ultrahigh-temperature ceramic nanocomposite with excellent mechanical properties and ablation resistance. Journal of Advanced Ceramics, 2025, 14(7): 9221104.
43. J B Huang, W Z Wang, Y J Li; et al. Improve durability of plasma-splayed thermal barrier coatings by decreasing sintering-induced stiffening in ceramic coatings[J].Journal of the European Ceramic Society, 2020, 40(4): 1433-1442.
44. J B Huang, X Chu, T Yang; et al. Achieving high anti-sintering performance of plasma-sprayed YSZ thermal barrier coatings through pore structure design[J]. Surface & Coatings Technology, 2022, 435: 128259.
45. Z H Xu, L M He, R D Mu; et al. Thermal cycling behavior of YSZ and La2(Zr0.7Ce0.3)2O7 as double-ceramic-layer systems EB-PVD TBCs[J]. Journal of Alloys and Compounds, 2012, 525: 87-96.
46. P Carpio, M Salvador, A Borrell; et al. Thermal behaviour of multilayer and functionally-graded YSZ/$Gd_2Zr_2O_7$ coatings[J]. Ceramics International, 2016, 43(5): 4048-4054.
47. B W Lv, X L Fan, D J Li; et al. Towards enhanced sintering resistance: Air-plasma-sprayed thermal barrier coating system with porosity gradient[J]. Journal of the European Ceramic Society, 2018, 38(4): 1946-1956.
48. S Arnal, S Fourcade, F Mauvy; et al. Design of a new yttrium silicate environmental barrier coating (EBC) based on the relationship between microstructure, transport properties and protection efficiency[J]. Journal of the European Ceramic Society, 2022, 42(3): 1061-1076.
49. K H Yang, J M Shi, F Q Tian; et al. Lanthanide co-doped YSZ double-ceramic-layer thermal barrier coatings: Unlocking superior sintering resistance, thermal durability, and insulation for extreme environments[J]. Surface & Coatings Technology, 2025, 504: 132069.
50. Civil Aviation University of China. Fabrication method of ceramic sealing coating with “brick-mud” layered structure: ZL 202111255442.7[P]. 2023-04-25.
51. T T Cheng, Z P Wang, S J Dai; et al. Fabrication of ceramic sealing coatings for shell bionic structures and their failure mechanism during thermal cycling[J]. Ceramics International, 2023, 49(06): 8962-8975.
52. T T Cheng, Y L Dong, L Ma; et al. Experiment and numerical simulation on thermal cycling performance of YSZ-based sealing coatings with “brick-mud” layered structure [J]. Coatings, 2024, 14(3): 14030351.
53. Civil Aviation University of China. Fabrication method of ceramic coating with tunable vertical cracks growth capability: ZL 202310420288.7[P]. 2025-06-20.
54. A Hospach, G Mauer, R Vaßen; et al. Characteristics of ceramic coatings made by thin film low pressure plasma spraying (LPPS-TF)[J]. Journal of Thermal Spray Technology, 2012, 21: 435-440.
55. S Kumar, B Dhas, D Roy. Emergence of pseudo-ductility in laminated ceramic composites[J]. Composite Structures, 2018, 204: 664-676.